Syntheses, Characterization, and in Vitro Degradation of Ethyl Cellulose-*graft*-poly(ϵ-caprolactone)-*block*-poly(L-lactide) Copolymers by Sequential Ring-Opening Polymerization

Weizhong Yuan,[†] Jinying Yuan,*[,†] Fengbo Zhang,[‡] and Xuming Xie[‡]

Key Lab of Organic Optoelectronics and Molecular Engineering of Ministry of Education, Department of Chemistry and Department of Chemical Engineering, Tsinghua University, Beijing 100084, People's Republic of China

Received October 17, 2006; Revised Manuscript Received December 11, 2006

Well-defined ethyl cellulose-*graft*-poly(ϵ-caprolactone) (EC-*g*-PCL) graft copolymers were successfully synthesized via ring-opening polymerization (ROP) of ϵ-caprolactone (CL) with an ethyl cellulose (EC) initiator and a tin 2-ethylhexanoate ($Sn(Oct)_2$) catalyst in xylene at 120 °C. Then, novel ethyl cellulose-*graft*-poly(ϵ-caprolactone)-*block*-poly(L-lactide) (EC-*g*-PCL-*b*-PLLA) graft-block copolymers were prepared by ROP of l-lactide (L-LA) with a hydroxyl-terminated EC-*g*-PCL macroinitiator and $Sn(Oct)_2$ catalyst in bulk at 120 °C. Various graft and block lengths of EC-*g*-PCL and EC-*g*-PCL-*b*-PLLA copolymers were obtained by adjusting the molar ratios of CL monomer to EC and the L-LA monomer to CL. The thermal properties and crystalline morphologies of EC-*g*-PCL and EC-*g*-PCL-*b*-PLLA copolymers were different from those of linear PCL. The in vitro degradation rate of EC-*g*-PCL-*b*-PLLA was faster than those of linear PCL and EC-*g*-PCL due to the presence of PLLA blocks.

Introduction

Considerable attention has been paid to aliphatic polyesters from lactones and lactides due to their excellent biodegradability, biocompatibility, and permeability. Among them, poly(ϵ-caprolactone) (PCL), poly(L-lactide) (PLLA), and their copolymers are especially interesting for their applications as biomedical materials, such as biodegradable sutures, drug delivery systems, and temporary scaffolds for tissue.[1−9] The effective synthesis method of polyesters is the ring-opening polymerization (ROP) of lactones and lactides.[10−16] Moreover, tin 2-ethylhexanoate ($Sn(Oct)_2$) is the widely used catalyst for the production of biodegradable polyesters due to the high yield, controlled molecular weight, and narrow distribution.[17−20] In addition, $Sn(Oct)_2$ can avoid transesterification reactions when used to produce copolyesters and also has a low biologic toxicity. Polyesters with well-defined architectures such as star-shaped polymers,[21−25] hyper-branched polymers,[26,27] dendrimers,[28−32] and comb-like polymers[33,34] are attracting increasing interest because they can modify the structural and physical properties of PCL and PLLA, which suffer from the lack of controlled degradation due to their high degree of crystallinity.[35,36]

Cellulose is the most abundant natural biomaterial in the world and presents good biocompatibility, biodegradability and renewability.[37−44] Modification of cellulose and its derivatives by graft copolymerization can provide a significant method to alter its physical and chemical properties.[45−52] Gupta and Khandekar prepared temperature-responsive cellulose by ceric ion-initiated graft copolymerization of *N*-isopropylacrylamide.[45] Nishio et al. investigated the enzymatic hydrolysis behavior, surface morphological characterization, and thermal and mechanical properties of cellulose diacetate-*graft*-poly(lactic acid)s.[46,47] Hult et al. reported the grafting of cellulose with poly(ϵ-caprolactone) and poly(L-lactide) via ROP.[48] Huang et al. reported the graft copolymer cellulose diacetate-*graft*-poly(methyl methacrylate) and ethyl cellulose-*graft*-polystyrene/poly(methyl methacrylate) by atom transfer radical polymerization.[49,50] Hafrén and Córdova synthesized the PCL by ROP with a cellulose initiator and organic acid catalyst.[51]

Scheme 1. Synthesis of EC-*g*-PCL-*b*-PLLA Graft-Block Copolymer

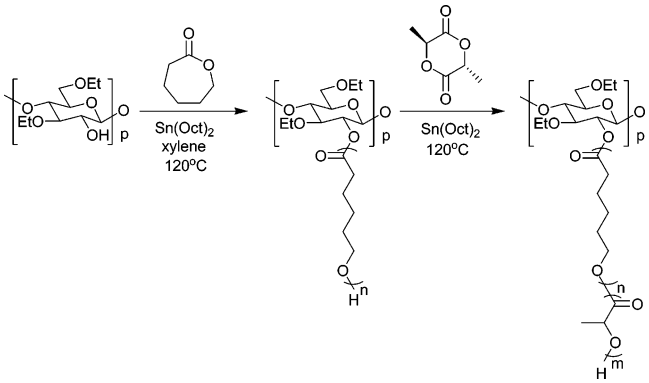

Ethyl cellulose (EC) is a kind of cellulose derivative that possesses good biocompatibility, high mechanical intensity, and stability.[53] Therefore, the work present here demonstrates the preparation of novel and well-defined graft-block copolymers based on the EC backbone. These unique copolymers could be used as biomaterials for their excellent biocompatible components. Moreover, the graft-block structure of copolymers and the different degradation rates of PCL segments and PLLA segments will produce controllable stepwise biodegradation properties. EC was used as an initiator for the ROP of CL in xylene to produce the ethyl cellulose-*graft*-poly(ϵ-caprolactone) (EC-*g*-PCL) graft copolymer. Then, the ethyl cellulose-*graft*-poly(ϵ-caprolactone)-*block*-poly(L-lactide) (EC-*g*-PCL-*b*-PLLA)

* Corresponding author. Tel.: +86 10 6278 3668; fax: +86 10 6277 1149; e-mail: yuanjy@mail.tsinghua.edu.cn.
[†] Department of Chemistry.
[‡] Department of Chemical Engineering.

10.1021/bm0610018 CCC: $37.00
Published on Web 02/28/2007

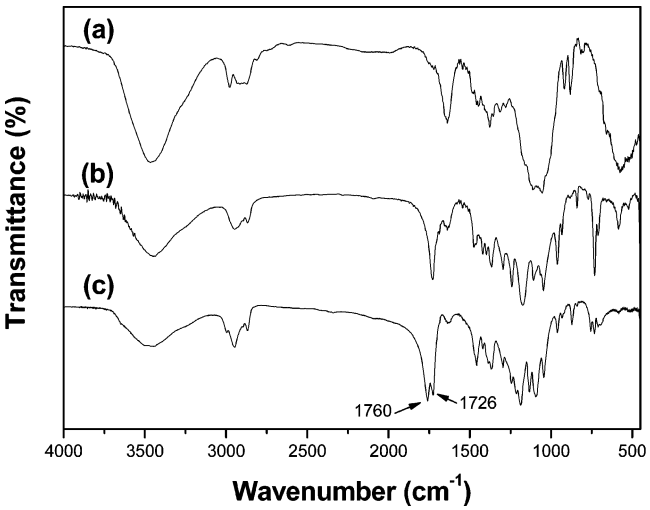

Figure 1. IR spectra of (a) EC, (b) EC-*g*-PCL graft copolymer, and (c) EC-*g*-PCL-*b*-PLLA graft-block copolymer.

Table 1. Preparation of Graft Copolymer CE-*g*-PCL and Graft-Block Copolymer CE-*g*-PCL-*b*-PLLA[a]

sample	[CL]/[LA]/[glucose unit of CE] (molar ratio)	$M_{n,NMR}$[b]	$M_{n,GPC}$[c]	M_w/M_n[c]
linear PCL		12 100	11 200	1.28
1	10:0:1	117 600	112 100	1.56
2	20:0:1	209 500	183 200	1.52
3	30:0:1	281 900	238 600	1.46
4	40:0:1	352 400	301 900	1.48
5	20:10:1	313 600	260 300	1.46
6	20:20:1	408 100	331 700	1.42
7	20:30:1	482 300	402 100	1.42
8	20:40:1	544 500	441 900	1.44

[a] Reaction conditions: [monomer]/[$Sn(Oct)_2$] = 1000, polymerization time = 24 h, and polymerization temperature = 120 °C. [b] $M_{n,NMR}$ was determined by ^1H NMR spectroscopy. [c] $M_{n,GPC}$ and M_w/M_n were determined by GPC analysis with polystyrene standards. THF was used as eluent.

graft-block copolymer was synthesized by ROP in bulk with the EC-*g*-PCL macroinitiator (Scheme 1).

The thermal properties of these polymers were investigated by DSC and TGA. Furthermore, the crystalline morphology of the polymers was observed by polarized optical microscopy (POM) and atomic force microscope (AFM). The in vitro degradation of the graft and graft-block copolymers was then studied.

Experimental Procedures

Materials. Ethyl cellulose (EC) (M_n = 19 000; the degree of ethyl substitution is 2.3) was obtained from Luzhou North Chemical Industry Co., Ltd. and was dried at 120 °C for 20 h under vacuum before use. ϵ-Caprolactone (Acros Organics) was purified with CaH_2 by vacuum distillation in a nitrogen atmosphere. L-Lactide (Purac Biochem) was purified by recrystallization from ethyl acetate twice and dried in a vacuum at room temperature. Tin 2-ethylhexanoate (Aldrich) was distilled under reduced pressure before use. Xylene and chloroform were dried over CaH_2 and distilled before use.

Characterization. ^1H NMR and ^{13}C NMR spectra were obtained from a JEOL JNM-ECA300 NMR spectrometer with $CDCl_3$ as a solvent. The chemical shifts were relative to tetramethylsilane at δ = 0 ppm for protons. Infrared spectra (FT-−IR) were recorded on an AVATAR 360 ESP FT-−IR spectrometer. The molecular weight and molecular weight distribution were measured on a Viscotek TDA 302 gel permeation chromatography machine equipped with two columns (GMHHR-H, M Mixed Bed). THF was used as eluent at a flow rate of 1 mL/min at 30 °C. Differential scanning calorimetric analysis (DSC) was carried out on a DSC 2910 thermal analysis system. Samples were first heated from −10 to 180 °C with a heating rate of 10 °C/min under nitrogen atmosphere and held for 3 min to erase the thermal history, then cooled to −10 °C at 5 °C/min, and finally heated to 180 °C at 10 °C/min. Thermogravimetric analysis (TGA) was carried on a TGA 2050 thermogravimetric analyzer with a heating rate of 20 °C/min from 20 to 600 °C under nitrogen atmosphere. The crystalline morphology of the polymer was observed using a XS-402 polarized optical microscope (Shanghai Microimage Technology). A solution of the sample in chloroform (8.9 mg/mL) was dropped to a glass plate under spin-coating at room temperature. The polymer films were placed at room temperature for 48 h to evaporate the solvent completely. Then, the films were heated to 100 °C for 3 h and quenched to 35 °C and maintained at this temperature for 60 h. The AFM images of the polymers were recorded on a SPM-9500J3 atomic force microscope (Shimadzu). The films on transparent mica substrate were obtained from spin-coating of the polymer solution, and the thickness was about 80 nm.

Synthesis of EC-*g*-PCL Copolymer. A typical polymerization procedure was shown as follows: EC (0.607 g, 31.9 μmol) was dissolved in 15 mL of freshly anhydrous xylene in a fire-dried polymerization tube. CL (6.08 g, 53.27 mmol), a catalytic amount of $Sn(Oct)_2$, and a dried magnetic stirring bar were added into the polymerization tube. The tube was then connected to a Schlenk line, where exhausting−refilling processes were repeated 3 times. The tube was immersed into an oil bath at 120 °C under nitrogen atmosphere with vigorous stirring for 24 h. After cooling to room temperature, the resulting polymer was dissolved in chloroform and precipitated 2 times with methanol and petroleum ether to afford the purified graft copolymer. The purified copolymer was dried in a vacuum oven until constant weight.

$M_{n,GPC}$ = 183 200, M_w/M_n = 1.52, IR (KBr, cm^{-1}): 3160−3670 (ν_{O-H}), 2952 (ν_{C-H}), 2866 (ν_{C-H}), 1730 ($\nu_{C=O}$). ^1H NMR ($CDCl_3$, δ, ppm): 4.05 (t, terminal CH_2O in PCL), 3.02−3.86 (protons on EC), 3.63 (t, terminal CH_2O in PCL), 2.29 (m, $COCH_2$ in PCL), 1.63 (m, $COCH_2$ in PCL), 1.38 (m, CH_2 in PCL), 1.14 (m, CH_3 in EC).

Synthesis of EC-*g*-PCL-*b*-PLLA Copolymer. A typical example is given next. The hydroxyl-terminated EC-*g*-PCL (0.61 g, 2.9 μmol), L-LA (0.70 g, 48.57 mmol), and a dried magnetic stirring bar were added to a fire-dried polymerization tube quickly. The tube was then connected to a Schlenk line, where exhausting−refilling processes were repeated 3 times. The tube was put into an oil bath at 120 °C with vigorous stirring for 5 min. A catalytic amount of $Sn(Oct)_2$ in anhydrous toluene was added to the melted mixture, and the exhausting−refilling process was carried out again to remove the toluene. The tube was put into an oil bath at 120 °C under nitrogen atmosphere with stirring and cooled to room temperature after polymerization for 24 h. The resulting product was dissolved in chloroform and precipitated 2 times with petroleum ether. The purified polymer was dried in a vacuum oven until constant weight.

$M_{n,GPC}$ = 331 700, M_w/M_n = 1.42, IR (KBr, cm^{-1}): 3180−3640 (ν_{O-H}), 2996 (ν_{C-H}), 2952 (ν_{C-H}), 2864 (ν_{C-H}), 1760 ($\nu_{C=O}$), 1726 ($\nu_{C=O}$). ^1H NMR ($CDCl_3$, δ, ppm): 5.16 (m, CH_3 in PLLA), 4.35 (t, terminal CHO in PLLA), 4.06 (m, CH_2O in PCL), 3.02−3.86 (protons on EC), 2.29 (m, $COCH_2$ in PCL), 1.56−1.63 (m, CH_2 in PCL and CH_3 in PLLA), 1.14 (m, CH_3 in EC). ^{13}C NMR ($CDCl_3$, δ, ppm): 173.7 (CO in PCL), 169.6 (CO in PLLA), 69.1 (CH in PLLA), 64.3 (CH_2O in PCL), 34.1 (CH_2 in PCL), 28.5 (CH_2 in PCL), 25.6 (CH_2 in PCL), 24.6 (CH_2 in PCL), 16.7 (CH_3 in PLLA).

In Vitro Degradation of Polymers. The films of linear PCL, EC-*g*-PCL, and EC-*g*-PCL-*b*-PLLA were cast from 6% chloroform solution (w/v). Residual solvents were removed in vacuo at room temperature until a constant weight was obtained. The thickness of the film was

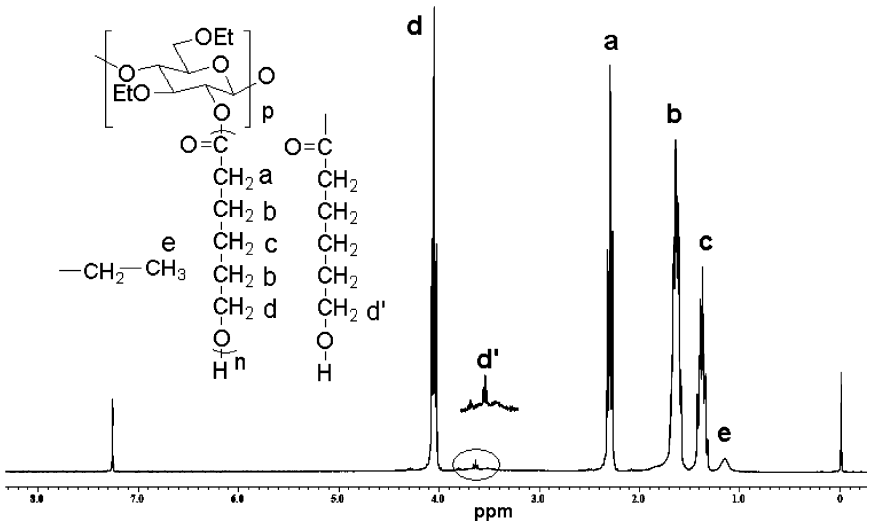

Figure 2. ^{1}H NMR spectrum of EC-*g*-PCL graft copolymer.

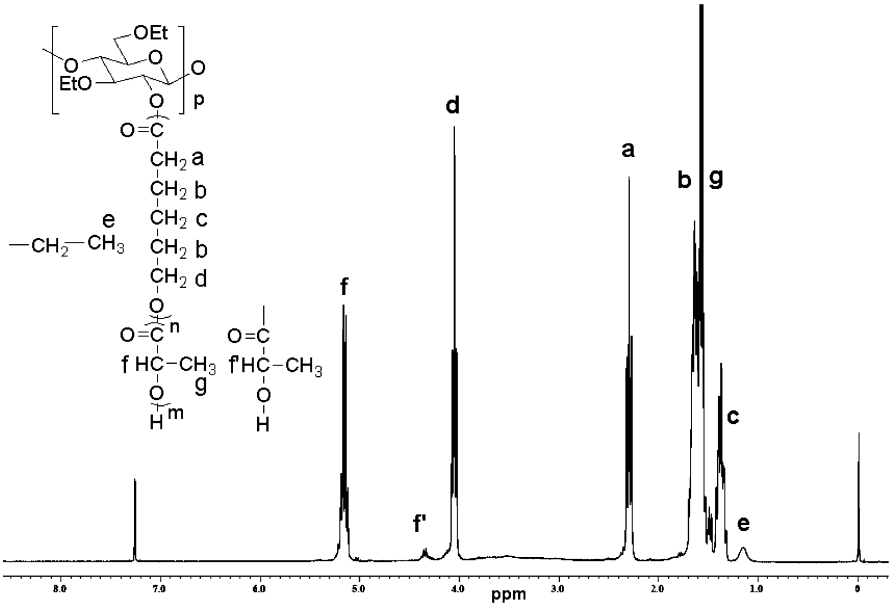

Figure 3. ^{1}H NMR spectrum of EC-*g*-PCL-*b*-PLLA graft-block copolymer.

found to be 0.2 mm. The films were placed in closed bottles containing phosphate buffered solution (PBS, pH 7.4) at 37 °C for 30 days. At given time intervals, the specimens were washed with distilled water and dried in vacuo to a constant weight at room temperature. The degradation was investigated by detecting weight loss.

Results and Discussion

Preparation of EC-*g*-PCL Copolymer. The graft polymerization of CL with EC was carried out in the presence of Sn(Oct)$_2$ as a catalyst and xylene as a solvent to afford the EC-*g*-PCL copolymer. The graft copolymerization reaction of cellulose was hindered under heterogeneous conditions, and homogeneous conditions were indispensable to the successful performance of polymerization to obtain comparative long graft polymer chains. EC possesses good solubility in common organic solvents such as chloroform, THF, xylene, etc. Therefore, a homogeneous ROP reaction of CL was successfully performed on the EC backbone in xylene because EC, CL, and EC-*g*-PCL could be dissolved in xylene. The IR spectrum of the EC-*g*-PCL copolymer is shown in Figure 1 b.

The wide peak at 3160−3670 cm^{-1} was the absorption band of the hydroxyl group of EC-*g*-PCL. As compared to the IR spectrum of EC (Figure 1 a), the absorption of the hydroxyl group of EC-*g*-PCL was decreased owing to polymerization, and a new absorption band at 1730 cm^{-1} assigned to the carbonyl band of PCL could be detected. A typical ^{1}H NMR spectrum of EC-*g*-PCL (sample 2) with assignments is shown in Figure 2.

The major resonance peaks a−d were attributed to PCL. The methylene proton signal (d′, $\delta = 3.63$ ppm) indicated that PCL was terminated by hydroxyl groups. To obtain graft copolymers with different molecular weights, the molar ratio of CL and glucose unit of CE were varied (CL)/[glucose unit of CE] = 10, 20, 30, and 40). The average polymerization degree of CL grafted on every glucose unit of the CE backbone was calculated from the ratio of the integral areas of the methylene signals of PCL at 2.29 ppm to the methyl protons signal of CE at 1.14 ppm (Table 1).

According to the data of the average polymerization degree and number-average molecular weights by GPC listed in Table 1, the residual free hydroxyl groups (seven hydroxyl groups

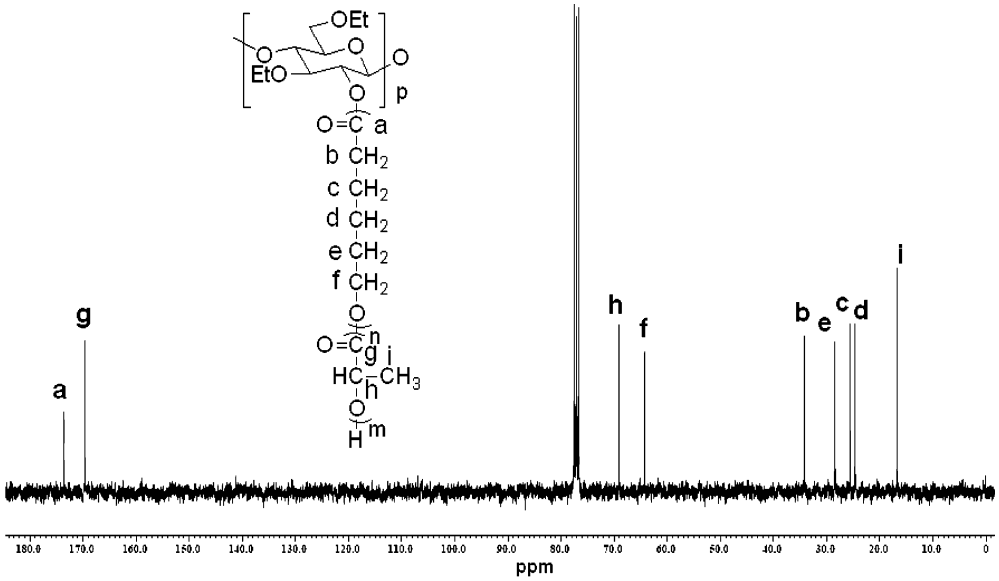

Figure 4. ^{13}C NMR spectrum of EC-*g*-PCL-*b*-PLLA graft-block copolymer.

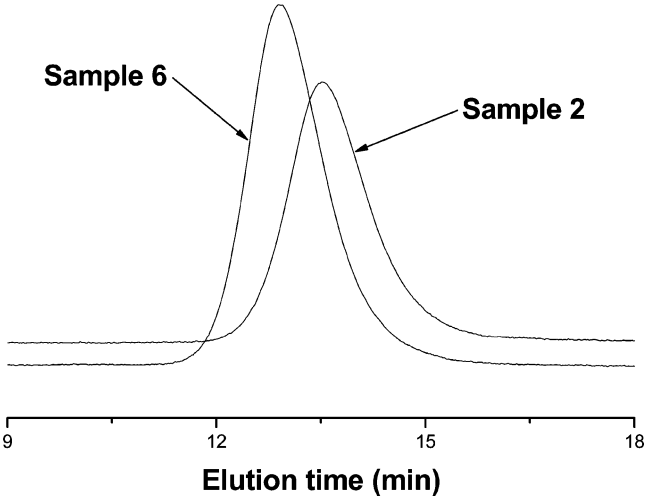

Figure 5. GPC traces of EC-*g*-PCL graft copolymer (sample 2) and EC-*g*-PCL-*b*-PLLA graft-block copolymer (sample 6).

per 10 glucose units) of the EC backbone could be used as effective propagation centers for the ROP of CL. All these indicated that the reaction conditions were beneficial for the penetration of CL molecules into the interior of EC, so the graft polymerization was easily initiated through the hydroxyl groups of the EC backbone.

Preparation of EC-*g*-PCL-*b*-PLLA Copolymer. The hydroxyl-terminated EC-*g*-PCL was used as a macroinitiator for the block copolymerization with L-LA in bulk using $Sn(Oct)_2$ as a catalyst. The IR spectrum of the EC-*g*-PCL-*b*-PLLA graft-block copolymer is shown in Figure 1c. The main difference in the IR spectrum between EC-*g*-PCL-*b*-PLLA and EC-*g*-PCL was the carbonyl absorption band region. In the IR spectrum of EC-*g*-PCL-*b*-PLLA, the carbonyl absorption band became wide and split into two peaks. The peak at 1760 cm^{-1} corresponded to the carbonyl absorption of PLLA units, while the peak at 1726 cm^{-1} was assigned to the carbonyl absorption of PCL units. It was important to prove that the PLLA chains existed in the copolymer as a block.[54,55] The ^1H NMR spectrum of EC-*g*-PCL-*b*-PLLA is shown in Figure 3.

The peak assigned to the methylene protons of the PCL block at 3.63 ppm disappeared, and a new peak at 4.35 ppm for the produced end group of the PLLA block was observed. This indicated that the terminal hydroxyl groups of the EC-*g*-PCL macroinitiator successfully initiated the polymerization of L-LA. The average polymerization degree of L-LA was also determined by the integration ratio of methine protons of the PLLA block at 4.35 ppm and the methylene protons of PCL at 2.29 ppm. The data of the average polymerization degree and number-average molecular weights by GPC (Table 1) demonstrated that the hydroxyl-terminated EC-*g*-PCL macroinitiator could initiate the ROP of L-LA. A typical ^{13}C NMR spectrum of EC-*g*-PCL-*b*-PLLA was shown in Figure 4.

This spectrum indicated that the graft-block copolymer did not present any intermediate signals between the carbonyl of PCL at 173.7 ppm and the carbonyl of PLLA at 169.6 ppm. Moreover, there was only one peak for each of the carbonyls. All these indicated that a transesterification reaction of PCL did not occur during the ROP of L-LA to obtain the graft-block copolymer EC-*g*-PCL-*b*-PLLA. The GPC traces of the graft copolymer EC-*g*-PCL (sample 2) and graft-block copolymer EC-*g*-PCL-*b*-PLLA (sample 6) are shown in Figure 5. These traces were monomodal, suggesting that these purified copolymers were pure graft or graft-block copolymers.

Thermal Properties of Polymers. The thermal properties of linear PCL, EC-*g*-PCL graft copolymer, and EC-*g*-PCL-*b*-PLLA graft-block copolymer were investigated by DSC and TGA, and the results are listed in Table 2. Figure 6 shows the DSC curves of these polymers in the first and second heating runs.

According to Table 2 and Figure 6, the melting point (T_m) and the degree of crystallinity (X_c) of EC-*g*-PCL were lower than those of linear PCL and increased with the length of the PCL graft chains, which should be attributed to the crystalline imperfection mainly due to the short chain length of PCL segments in graft copolymers. Moreover, the branched structure of these polymers should make a contribution to the imperfections. Furthermore, the EC backbone was an amorphous polymer, and the presence of EC in the copolymer could hinder the crystallization of PCL segments. In the EC-*g*-PCL graft copolymer, the chain movements of the PCL branches were hindered, and their crystallization ability was weakened. The EC-*g*-PCL-*b*-PLLA graft-block copolymer showed a double melting peak, reflecting the presence of two crystalline domains. Moreover, the values of T_m and X_c of the PCL block in EC-*g*-

Table 2. Thermal Properties of Graft Copolymer EC-*g*-PCL and Graft-Block Copolymer EC-*g*-PCL-*b*-PLLA

	T_m (°C)[a]		ΔH_m (J/g)[b]		X_c (%)[c]			
sample[d]	T_{m1}	T_{m2}	ΔH_{m1}	ΔH_{m2}	X_{c1}	X_{c2}	T_{onset} (°C)[e]	T_{max} (°C)[f]
linear PCL	61.9	57.1	86.5	67.7	63.6	49.7	338.1	372.8
1	58.6	52.4	62.0	43.1	45.6	31.7	303.9	329.8
2	60.7	54.3	80.9	56.3	59.4	41.4	309.3	336.3
3	60.9	55.3	81.8	57.6	60.1	42.3	313.5	339.9
4	61.1	55.6	82.3	58.2	60.5	42.8	316.6	342.6
5	57.2, 160.4	48.9, 158.3	50.1, 10.3	34.4, 9.1	36.8, 11.0	25.3, 9.7	230.8	268.3
6	55.8, 163.8	50.0, 162.4	33.5, 15.3	26.3, 14.8	24.6, 16.3	19.3, 15.8	235.3	272.4
7	46.0 164.1	44.7, 163.2	27.3, 17.6	15.7, 15.9	20.1, 18.8	11.5, 17.0	237.1	276.6
8	45.6, 164.8	44.5, 163.6	17.6, 20.1	11.4, 17.6	12.9, 21.5	8.4, 18.8	239.8	278.7

[a] T_m denotes the melting point of PCL and PLLA segments. [b] Heat of melting crystalline PCL and PLLA segments. [c] The degree of crystalline PCL and PLLA segments. Calculated from the heat of melting using the melting of 136.1 J/g of 100% crystalline PCL and 93.6 J/g of 100% crystalline PLLA. [d] Samples are the same as Table 1. [e] T_{onset} is the onset decomposition temperature. [f] T_{max} is the temperature corresponding to the maximum rate of weight loss.

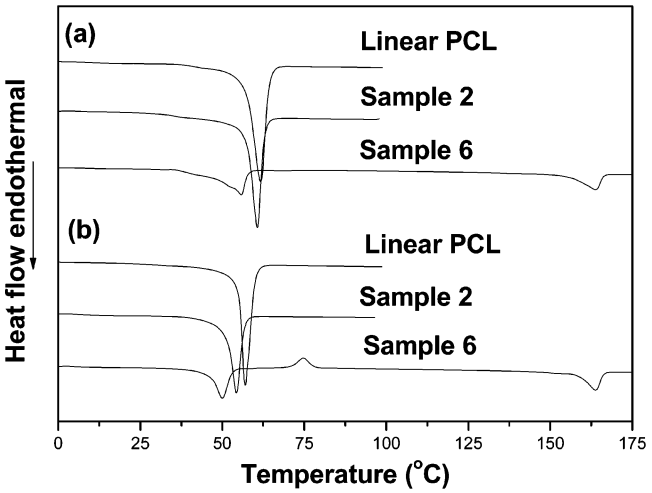

Figure 6. DSC curves of linear PCL, EC-*g*-PCL graft copolymer (sample 2), and EC-*g*-PCL-*b*-PLLA graft-block copolymer (sample 6) in the first heating run (a) and in the second heating run (b), respectively.

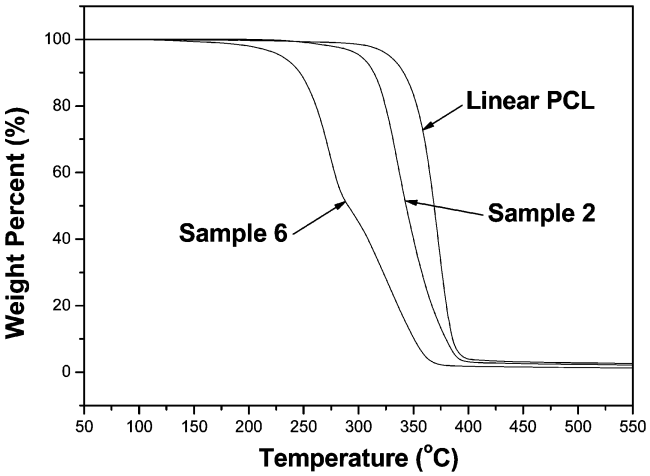

Figure 7. TGA thermograms of linear PCL, EC-*g*-PCL graft copolymer (sample 2), and EC-*g*-PCL-*b*-PLLA graft-block copolymer (sample 6).

PCL-*b*-PLLA decreased with an increase of the length of the PLLA block and were obviously lower than those of the linear PCL and PCL segments in graft copolymers. This suggested that the crystallization of PCL block was restricted by the crystallized PLLA block. Meanwhile, the crystallization of the PLLA block was also restricted by the crystallized PCL block. These results indicated that the crystallization of both the PCL and the PLLA blocks mutually interfered with each other. At the same time, the values of T_m and X_c of the PCL and PLLA segments of polymers in the second heating run were lower than those in the first heating run. For example, the values of T_m and X_c of sample 2 were 54.3 °C and 41.4% determined in the second run, respectively. However, the values were 60.7 °C and 59.4% determined in the first run, respectively. This phenomenon could be explained as follows: the sample was first melted in the process of heating. Then, the sample was quenched to −10 °C at a comparatively rapid rate after erasing the thermal history. Therefore, the crystallizable segments in the polymer did not have enough time to form a comparative perfect crystal structure. Furthermore, the data of TGA also demonstrated that the onset decomposition temperature (T_{onset}) and the maximum decomposition temperature (T_{max}) of EC-*g*-PCL were lower than those of the linear one. With the increase of the length of the PCL segments in the copolymer, the increase of T_{onset} and T_{max} occurred. It can be seen from Table 2 and Figure 7 that T_{onset} and T_{max} of linear PCL were 338.1 and 372.8 °C, respectively. However, T_{onset} and T_{max} of EC-*g*-PC (sample 2) were 309.3 and 336.3 °C, respectively. The relatively poor thermal stability of EC-*g*-PCL with short PCL chains than linear PCL and EC-*g*-PCL with long PCL chains could be ascribed to the increase of thermally unstable hydroxyl groups of the polymer. As shown in Figure 7, T_{onset} and T_{max} of EC-*g*-PCL-*b*-PLLA (sample 6) were 235.3 and 272.4 °C, respectively, and different from those of EC-*g*-PCL. This can be attributed to the poorer thermal stability of the PLLA segments than that of the PCL segments in EC-*g*-PCL.

Crystalline Morphologies of Polymers. The crystalline morphologies of linear PCL, EC-*g*-PCL graft copolymer (sample 2), and EC-*g*-PCL-*b*-PLLA graft-block copolymer (sample 6) were investigated by polarized optical micrographs. As shown in Figure 8, the polarized optical micrographs of linear PCL and sample 2 were obtained from films after annealing, while the polarized optical micrograph of sample 6 was gained from the film before and after annealing. According to Figure 8, linear PCL showed a typical spherulitic morphology. Maltese cross patterns could be obviously observed in linear PCL.

As compared to linear PCL, EC-*g*-PCL presented a more complicated spherulitic morphology, namely, Maltese cross patterns along with band textures. The formation of banded spherulites in the EC-*g*-PCL copolymer was related to a uniform average twisting of the lamellae along the radius orientation of the PCL spherulites, which should be attributed to the presence of amorphous EC microregions in the graft copolymer interfer-

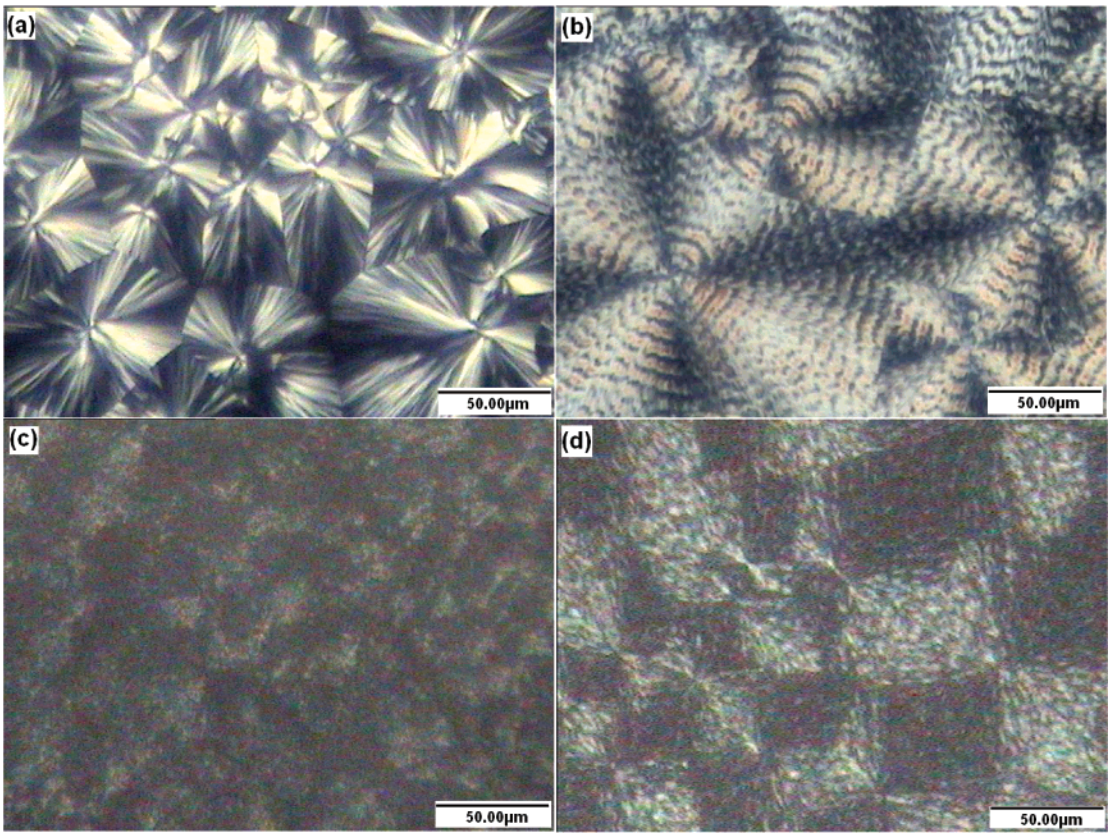

Figure 8. Polarized optical micrographs of (a) linear PCL, (b) EC-*g*-PCL graft copolymer (sample 2), (c) EC-*g*-PCL-*b*-PLLA graft-block copolymer (sample 6) (after annealing), and (d) EC-*g*-PCL-*b*-PLLA graft-block copolymer (sample 6) (before annealing).

ing with the natural growth of spherulites. The crystalline morphology of the EC-*g*-PCL-*b*-PLLA graft-block copolymer was different from that of linear PCL and the EC-*g*-PCL graft copolymer. Before annealing, the graft-block copolymer presented banded and imperfect spherulites (papilionaceous patterns) with no obvious Maltese cross patterns. The result could be attributed to the presence of amorphous EC microregions and the mixed spherulites of both PCL and PLLA blocks, leading to the twisting of lamellae and the formation of imperfect spherulites. When the graft-block copolymer was heated to 100 °C, where the temperature was higher than the melting point of the PCL blocks but much lower than that of the PLLA blocks, the crystals of the PLLA blocks were not destroyed. The microregions of EC and PLLA seriously hindered the natural growth of the PCL spherulites at 35 °C. The crystallization of the PCL segments was mainly templated by the existing PLLA crystals and EC microregions. Therefore, the annealing process resulted in the formation of imperfect crystals. Notably, the crystalline morphologies of the EC-*g*-PCL graft copolymer and EC-*g*-PCL-*b*-PLLA graft-block copolymer were different from spherulites with Maltese cross patterns of linear PCL.

AFM images were used to further confirm the different crystalline morphologies of polymers with different structures. The AFM height images of EC, linear PCL, EC-*g*-PCL, and EC-*g*-PCL-*b*-PLLA are shown in Figure 9.

Figure 9a is the image of EC. The film was uniform and continuous, and EC could not be discerned from the image, which further confirmed that EC was an amorphous polymer. As shown in Figure 9b, the spherulites were large and perfect for linear PCL, which indicated that linear PCL possessed good crystallization ability. According to the image of EC-*g*-PCL (Figure 9c), the spherulites were smaller and less perfect than those of linear PCL, which could be ascribed to the branched structure and the presence of EC inducing the decrease of the crystallization ability of EC-*g*-PCL. As compared to linear PCL and EC-*g*-PCL, the spherulites of EC-*g*-PCL-*b*-PLLA (Figure 9d) were imperfect and tiny, which could be attributed to the interference of PCL and PLLA blocks leading to further weakening of the crystallization ability. All these conditions are in agreement with the results of the DSC measurement.

In Vitro Degradation of Polymers. The degradation behaviors of linear PCL, EC-*g*-PCL (sample 2), and EC-*g*-PCL-*b*-PLLA (sample 6) were investigated by immersing them in pH 7.4 PBS maintained at 37 °C. The weight losses of these polymers during the degradation period are shown in Figure 10.

The degradation rate of linear PCL was very slow. For example, the weight loss was only 2.1% after degradation for 30 days. This was attributed to it being a highly crystalline polymer with a degree of crystallinity of about 49.7%. The degradation rate of sample 2 was obviously faster than that of linear PCL. This could be ascribed to the branched structure of EC-*g*-PCL and shorter PCL chains than that of linear PCL, which resulted in a lower degree of crystallinity of EC-*g*-PCL (sample 2: $X_c = 41.4\%$). It was reported that the degradation of polyesters began in the amorphous zone and then the crystalline zone. Therefore, the degradation rate of sample 2 was faster than that of linear PCL. The degradation rate of EC-*g*-PCL-*b*-PLLA was faster than that of EC-*g*-PCL. To sample 6, the weight loss was 6.6% after degradation for 30 days. This should be attributed to the presence of PLLA blocks in the copolymer. During the degradation process, the water molecule pervaded the molecule of PLLA much faster than those of PCL because the content of the hydrolyzable ester

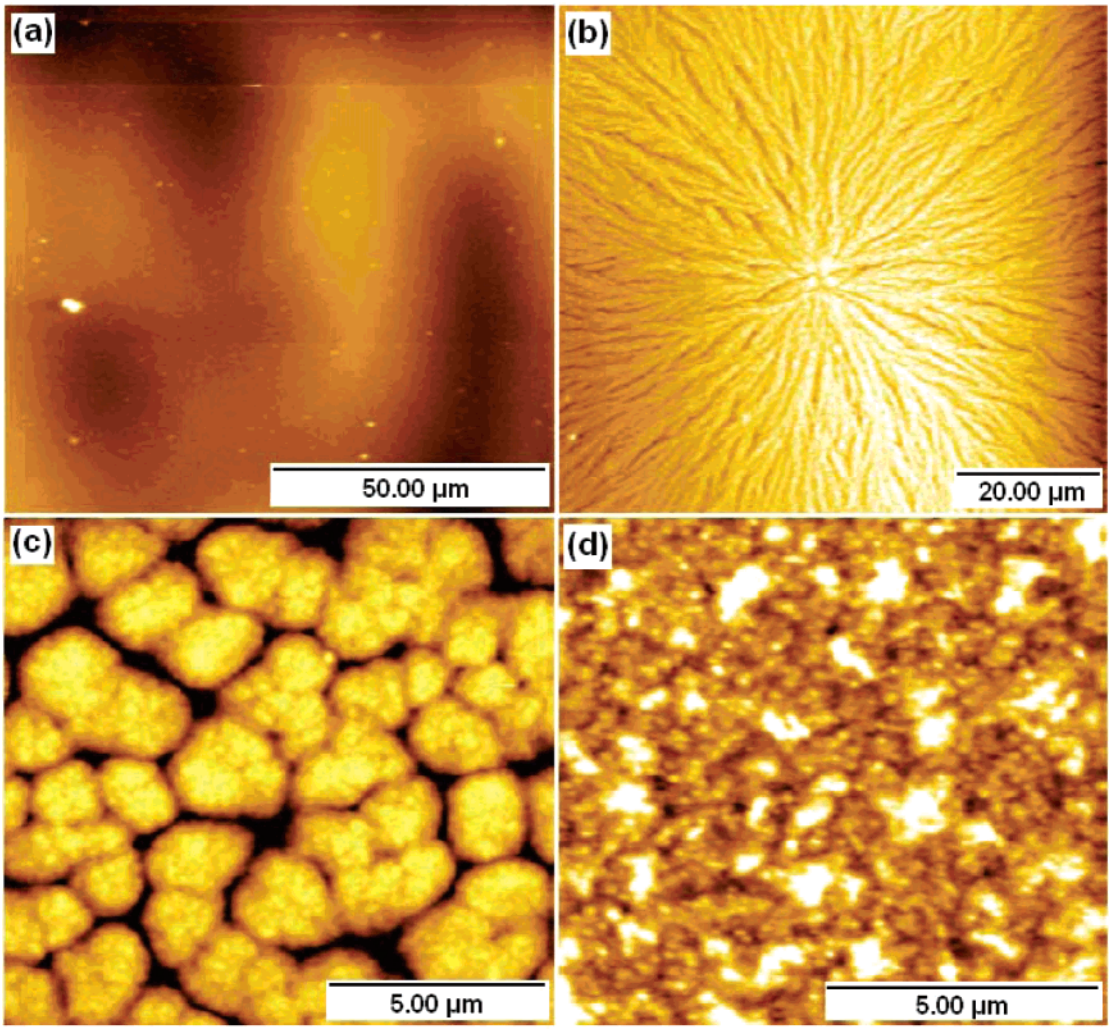

Figure 9. AFM height images of (a) EC, (b) linear PCL, (c) EC-*g*-PCL graft copolymer (sample 2), and (d) EC-*g*-PCL-*b*-PLLA graft-block copolymer (sample 6).

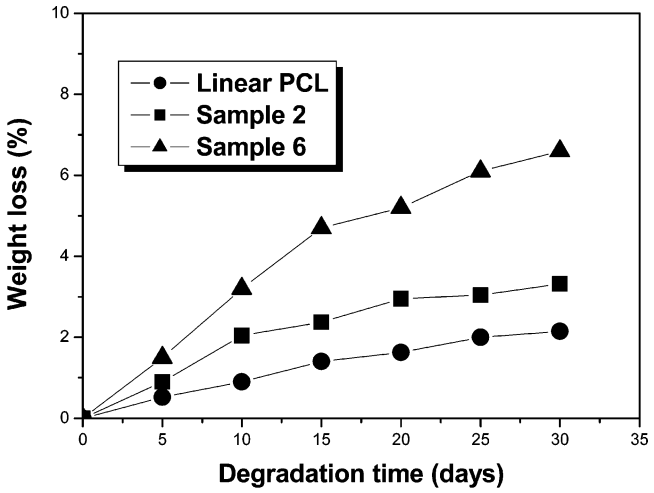

Figure 10. Degradation behaviors of linear PCL, EC-*g*-PCL graft copolymer (sample 2), and EC-*g*-PCL-*b*-PLLA graft-block copolymer (sample 6) in phosphate buffer solution (PBS, pH 7.4) at 37 °C.

groups in the PLLA segments was more than that in the PCL segments. Moreover, the PLLA segments possessed a lower crystalline degree than that of the PCL segments. Therefore, the degradation of the PLLA blocks was easier than that of the PCL blocks.

Conclusion

A series of novel EC-*g*-PCL graft copolymers and EC-*g*-PCL-*b*-PLLA graft-block copolymers was successfully prepared. The EC-*g*-PCL graft copolymer was synthesized by living ROP of CL in the presence of an EC initiator and $Sn(Oct)_2$ catalyst in xylene at 120 °C. Subsequently, the EC-*g*-PCL-*b*-PLLA graft-block copolymer was synthesized by ROP in bulk with an EC-*g*-PCL macroinitiator. Various graft and block lengths of EC-*g*-PCL and EC-*g*-PCL-*b*-PLLA were obtained by adjusting the molar ratios of the CL monomer to EC and the L-LA monomer to CL. The values of T_m and X_c of EC-*g*-PCL were enhanced with the increase of the length of PCL. To EC-*g*-PCL-*b*-PLLA, the T_m and X_c of the PLLA block increased with the increase of the length of PLLA. The thermal stability of EC-*g*-PCL with short PCL branches was poorer than that of linear PCL and EC-*g*-PCL with long PCL branches. Moreover, the thermal stability of EC-*g*-PCL-*b*-PLLA was poorer than that of EC-*g*-PCL. Furthermore, EC-*g*-PCL and EC-*g*-PCL-*b*-PLLA revealed crystalline morphologies that were different from that of linear PCL. The in vitro degradation rate of EC-*g*-PCL-*b*-PLLA was faster than that of linear PCL and EC-*g*-PCL due to the presence of PLLA blocks.

Acknowledgment. The authors gratefully acknowledge the financial support of the National Natural Science Foundation of China (50373023 and 20574042).

CDV

References and Notes

(1) Bisht, K. S.; Deng, F.; Gross, R. A.; Kaplan, D. L.; Swift, G. *J. Am. Chem. Soc.* **1998**, *120*, 1363−1367.
(2) Ko, B. T.; Liu, C. C. *J. Am. Chem. Soc.* **2001**, *123*, 7973−7977.
(3) O'Keefe, B. J.; Monnier, S. M.; Hillmyer, M. A.; Tolman, W. B. *J. Am. Chem. Soc.* **2001**, *123*, 339−340.
(4) Li, W. J.; Danielson, K. G.; Alexander, P. G.; Tuan, R. S. *J. Biomed. Mater. Res.* **2003**, *67*, 1105−1114.
(5) Brostrom, J.; Boss, A.; Chronakis, I. S. *Biomacromolecules* **2004**, *5*, 1124−1134.
(6) Wang, C. H.; Hsiue, G. H. *Bioconjugate Chem.* **2005**, *16*, 391−396.
(7) Wang, F.; Bronich, T. K.; Kabanov, A. V.; Rauh, R. D.; Roovers, J. *Bioconjugate Chem.* **2005**, *16*, 397−405.
(8) Ho, M. H.; Hou, L. T.; Tu, C. Y.; Hsieh, H. J.; Lai, J. Y.; Chen, W. J.; Wang, D. M. *Macromol. Biosci.* **2006**, *6*, 90−98.
(9) Meng, F. L.; Zheng, S. X.; Zhang, W. A.; Li, H. Q.; Liang, Q. *Macromolecules* **2006**, *39*, 711−719.
(10) Ni, Q.; Yu, L. *J. Am. Chem. Soc.* **1998**, *120*, 1645−1646.
(11) Deng, F.; Bisht, K. S.; Gross, R. A.; Kaplan, D. L. *Macromolecules* **1999**, *32*, 5159−5161.
(12) Chen, H.-Y.; Huang, B.-H.; Lin, C.-C. *Macromolecules* **2005**, *38*, 5400−5405.
(13) Cayuela, J.; Bounor-Legare, V.; Cassagnau, P.; Michel, A. *Macromolecules* **2006**, *39*, 1338−1346.
(14) Hsueh, M.-L.; Huang, B.-H.; Wu, J.; Lin, C.-C. *Macromolecules* **2005**, *38*, 9482−9487.
(15) Albertsson, A.-C.; Varma, I. K. *Biomacromolecules* **2003**, *4*, 1466−1486.
(16) Karikari, A. S.; Edwards, W. F.; Mecham, J. B.; Long, T. E. *Biomacromolecules* **2005**, *6*, 2866−2874.
(17) Dechy-Cabaret, O.; Martin-Vaca, B.; Bourissou, D. *Chem. Rev.* **2004**, *104*, 6147−6176.
(18) Rieger, J.; Coulembier, O.; Dubois, P.; Bernaerts, K. V.; Du Prez, F. E.; Jerome, R.; Jerome, C. *Macromolecules* **2005**, *38*, 10650−10657.
(19) Kowalski, A.; Libiszowski, J.; Biela, T.; Cypryk, M.; Duda, A.; Penczek, S. *Macromolecules* **2005**, *38*, 8170−8176.
(20) Deng, C.; Rong, G. Z.; Tian, H. Y.; Tang, Z. H.; Chen, X. S.; Jing, X. B. *Polymer* **2005**, *46*, 653−659.
(21) Tao, L.; Luan, B.; Pan, C. Y. *Polymer* **2003**, *44*, 1013−1020.
(22) Dong, C. M.; Qiu, K. Y.; Gu, Z. W.; Feng, X. D. *Macromolecules* **2001**, *34*, 4691−4696.
(23) Wang, J. L.; Wang, L.; Dong, C. M. *J. Polym. Sci., Part A: Polym. Chem.* **2005**, *43*, 5449−5457.
(24) Finne, A.; Albertsson, A.-C. *Biomacromolecules* **2002**, *3*, 684−690.
(25) Cai, C.; Wang, L.; Dong, C. M. *J. Polym. Sci., Part A: Polym. Chem.* **2005**, *44*, 2034−2044.
(26) Trollsas, M.; Atthoff, B.; Claesson, H.; Hedrick, J. L. *Macromolecules* **1998**, *31*, 3439−3445.
(27) Gottschalk, C.; Frey, H. *Macromolecules* **2006**, *39*, 1719−1723.
(28) Trollsas, M.; Hedrick, J. L. *J. Am. Chem. Soc.* **1998**, *120*, 4644−4651.
(29) Hedrick, J. L.; Trollsas, M.; Hawker, C. J.; Atthoff, B.; Claesson, H.; Heise, A.; Miller, R. D.; Mecerreyes, D.; Jerome, R.; Dubois, P. *Macromolecules* **1998**, *31*, 8691−8705.
(30) Cai, Q.; Zhao, Y.; Bei, J. Z.; Xi, F.; Wang, S. G. *Biomacromolecules* **2003**, *4*, 828−834.
(31) Yuan, W. Z.; Yuan, J. Y.; Mi, Z.; Sui, X. F. *J. Polym. Sci., Part A: Polym. Chem.* **2006**, *44*, 6575−6586.
(32) Zhao, Y.; Shuai, X.; Chen, C.; Xi, F. *Chem. Mater.* **2003**, *15*, 2836−2843.
(33) Ydens, I.; Rutot, D.; Degee, P.; Six, J.-L.; Dellacherie, E.; Dubois, P. *Macromolecules* **2000**, *33*, 6713−6721.
(34) Rieger, J.; Dubois, P.; Jerome, R.; Jerome, C. *Langmuir* **2006**, *22*, 7471−7479.
(35) Persenaire, O.; Alexandre, M.; Degee, P.; Dubois, P. *Biomacromolecules* **2001**, *2*, 288−294.
(36) Kikkawa, Y.; Abe, H.; Iwata, T.; Inoue, Y.; Doi, Y. *Biomacromolecules* **2002**, *3*, 350−356.
(37) Sturcova, A.; His, I.; Apperley, D. C.; Sugiyama, J.; Jarvis, M. C. *Biomacromolecules* **2004**, *5*, 1333−1339.
(38) Hinterstoisser, B.; Akerholm, M.; Salmen, L. *Biomacromolecules* **2003**, *4*, 1232−1237.
(39) Zhang, L.; Liu, H.; Zheng, L.; Zhang, J.; Du, Y.; Feng, H. *Ind. Eng. Chem. Res.* **1996**, *35*, 4682−4685.
(40) Turner, M. B.; Spear, S. K.; Holbrey, J. D.; Rogers, R. D. *Biomacromolecules* **2004**, *5*, 1379−1384.
(41) Beck-Candanedo, S.; Roman, M.; Gray, D. G. *Biomacromolecules* **2005**, *6*, 1048−1054.
(42) Cranston, E. D.; Gray, D. G. *Biomacromolecules* **2006**, *7*, 2522−2530.
(43) Wada, M.; Heux, L.; Sugiyama, J. *Biomacromolecules* **2004**, *5*, 1385−1391.
(44) Liu, J.; Wang, J.; Bachas, L. G.; Bhattacharyya, D. *Biotechnol. Prog.* **2001**, *17*, 866−871.
(45) Gupta, K. C.; Khandekar, K. *Biomacromolecules* **2003**, *4*, 758−765.
(46) Teramoto, Y.; Nishio, Y. *Biomacromolecules* **2004**, *5*, 407−414.
(47) Teramoto, Y.; Nishio, Y. *Polymer* **2003**, *44*, 2701−2709.
(48) Lonnberg, H.; Zhou, Q.; Brumer, H., III; Teeri, T. T.; Malmstrom, E.; Hult, A. *Biomacromolecules* **2006**, *7*, 2178−2185.
(49) Shen, D. W.; Huang, Y. *Polymer* **2004**, *45*, 7091−7097.
(50) Shen, D. W.; Yu, H.; Huang, Y. *J. Polym. Sci., Part A: Polym. Chem.* **2005**, *43*, 4099−4108.
(51) Hafrén, J.; Córdova, A. *Macromol. Rapid Commun.* **2005**, *26*, 82−86.
(52) Vlèek, P.; Janata, M.; Látalová, P.; Krí_, J.; Èadová, E.; Toman, L. *Polymer* **2006**, *47*, 2587−2595.
(53) Gupta, K. C.; Sahoo, S. *Biomacromolecules* **2001**, *2*, 239−247.
(54) Cai, Q.; Bei, J. Z.; Wang, S. G. *Polym. Adv. Technol.* **2000**, *11*, 159−166.
(55) Yuan, W. Z.; Tang, X. Z.; Huang, X. B.; Zheng, S. X. *Polymer* **2005**, *46*, 1701−1707.

BM0610018